Award Number: W81XWH-10-1-0864

TITLE: A Clinically Realistic Large Animal Model of Intra-Articular Fracture

PRINCIPAL INVESTIGATOR: Yuki Tochigi, M.D., Ph.D.

CONTRACTING ORGANIZATION: The University of Iowa
Iowa City, IA 52242

REPORT DATE: October 2012

TYPE OF REPORT: Annual

PREPARED FOR: U.S. Army Medical Research and Materiel Command
Fort Detrick, Maryland 21702-5012

DISTRIBUTION STATEMENT:

Approved for public release; distribution unlimited

REPORT DOCUMENTATION PAGE

Form Approved
OMB No. 0704-0188

1. REPORT DATE *(DD-MM-YYYY)*	2. REPORT TYPE	3. DATES COVERED *(From - To)*
1 October 2012	Annual	15 Sep 2011 - 14 Sep 2012

4. TITLE AND SUBTITLE
A Clinically Realistic Large Animal Model of Intra-Articular Fracture

5a. CONTRACT NUMBER
W81XWH-10-1-0864

5b. GRANT NUMBER

5c. PROGRAM ELEMENT NUMBER

6. AUTHOR(S)
Yuki Tochigi, M.D., Ph.D.

yuki-tochigi@uiowa.edu

5d. PROJECT NUMBER

5e. TASK NUMBER

5f. WORK UNIT NUMBER

7. PERFORMING ORGANIZATION NAME(S) AND ADDRESS(ES)
University of Iowa
Iowa City, Iowa 522452-1100

8. PERFORMING ORGANIZATION REPORT NUMBER

9. SPONSORING / MONITORING AGENCY NAME(S) AND ADDRESS(ES)
U.S. Army Medical Research and
Materiel Command, Fort Detrick,
Maryland 21702-5012

10. SPONSOR/MONITOR'S ACRONYM(S)

11. SPONSOR/MONITOR'S REPORT NUMBER(S)

12. DISTRIBUTION / AVAILABILITY STATEMENT
Approved for public release; distribution unlimited

13. SUPPLEMENTARY NOTES

14. ABSTRACT
The primary objective of this project is to develop a novel large animal survival model of intra-articular fracture (IAF) in which all major pathophysiological attributes of corresponding human clinical injuries are realistically replicated, and in which post-traumatic osteoarthritis (OA) predictively develops. Work during the reporting period (Year 1) has yielded definitive protocols to create a large animal survival IAF model and to document/analyze the natural course of fractured experimental joints in this model. In PY-3, documentation/analysis of the natural course data will be continued. Simultaneously, using the protocols established in the last two project years, the 7-day survival study to test the effect of a therapeutic treatment will be pursued.

15. SUBJECT TERMS
post-traumatic osteoarthritis, joint injuries, intra-articular fracture, survival animal model, cartilage degeneration

16. SECURITY CLASSIFICATION OF:			17. LIMITATION OF ABSTRACT	18. NUMBER OF PAGES	19a. NAME OF RESPONSIBLE PERSON
a. REPORT	b. ABSTRACT	c. THIS PAGE			USAMRMC
U	U	U	UU	40	19b. TELEPHONE NUMBER *(include area code)*

Table of Contents

Appendix (28 pages):

Tochigi, Y, Zhang, P, Rudert, MJ, et al. A novel impaction technique to create experimental articular fractures in large animal joints. Osteoarthritis Cartilage (in print).

1. INTRODUCTION

The primary objective of this project is to develop a novel large animal survival model of intra-articular fracture (IAF) in which all major pathophysiological attributes of corresponding human clinical injuries are realistically replicated, and in which post-traumatic osteoarthritis (OA) predictably develops. Specifically, work has been proposed to thoroughly validate the fracture insult technique/system developed for introducing pathophysiologically realistic IAFs in the porcine hock *in vivo* (Aim 1), to establish post-insult management methodology (Aim 2), and to validate the capability of the animal model as a research tool for piloting new treatment methods (Aim 3). At the conclusion of the project, we expect to have established a definitive methodology to create a clinically realistic large animal survival model of IAF, and we expect to have demonstrated the value of the animal model as a powerful new translational research tool. This animal model will facilitate translational research of orthopaedic treatment for IAFs, specifically by providing opportunities to test efficacy and safety of new treatment strategies prior to clinical trial, advancing orthopaedic treatment to mitigate the risk of OA following IAFs.

As documented in the last progress report, our work in the Project Year 1 (PY-1) yielded an established definitive impaction insult protocol to created experimental IAFs in the porcine hock *in vivo* (Aim 1). Using this insult protocol, in the reporting period (PY-2), we moved ahead to establish the definitive modeling protocol (Task 2 in the SOW), and to collect data to document the natural course of the novel animal IAF model in the mid-term survival study (Task 3). For these purposes, to date, a total of eighteen animals have been tested in three series of survival experiment. (Note: Six animals in the latest series are still in the process of testing.)

2. BODY

2.1 Modeling Protocol

2.1.a Fracture insult

Under general anesthesia, each animal is subjected to a fracture insult to the left hock (Figure 1), using the purpose-designed "off-set" impaction technique.[3] The experimental (left) joint is mounted on the custom pendulum-based impaction apparatus for delivering an impaction force pulse.[1] (As noted in the PY-1 annual report, this apparatus is equipped with instrumentation for measurement of energy absorption during fracture impaction.) The distal tibial shaft of the experimental leg is secured at a posteriorly tilted "offset" position, with a transverse stress-rising saw-cut (to guide the location and orientation of fracture line) placed across the anterior cortex, leaving a 5 mm-thick zone of juxta-articular bone intact. The distal impact face is anchored to the talus using three "tripod" pins, for direct (i.e., no soft tissue intervention) delivery of a fracture force pulse to the experimental joint. The force pulse is then delivered using a 5.8 kg pendulum mass dropped from a user-controlled height (currently 79 cm, to generate 45 joules of kinetic energy). The magnitude of energy absorption during the impaction insult is determined by measuring the difference between energy delivered (the pendulum's kinetic energy immediately before impaction) and energy passed through the specimen (energy transmitted to the sled-spring instrument to which the tibia holder is mounted).

Of the 18 animals tested to date, experimental fractures have been successfully created by a single impaction in 13 animals and after a repeated impaction in 3. Energy absorption during the impaction insult was 11.7 to 28.3 joules (mean $\pm$ SD: 21.3 $\pm$ 4.4). In every case, the fracture created was a transverse fracture with a large anterior malleolar fragment (Figure 2), which was morphology very consistent with those created in previous cadaver pilot work (Figure 3).

In the first two testing series, we have experienced two complication cases. The very first case required four repetitive impactions, with the energy delivery gradually increased until the fracture threshold was reached. The other case could not be successfully impacted due to malalignment of the bone anchorage device. After these experiences, we have made several technical refinements, and the latest (ongoing) testing series has achieved 100% success in fracture creation (6 out of 6 animals), all by a single impaction.

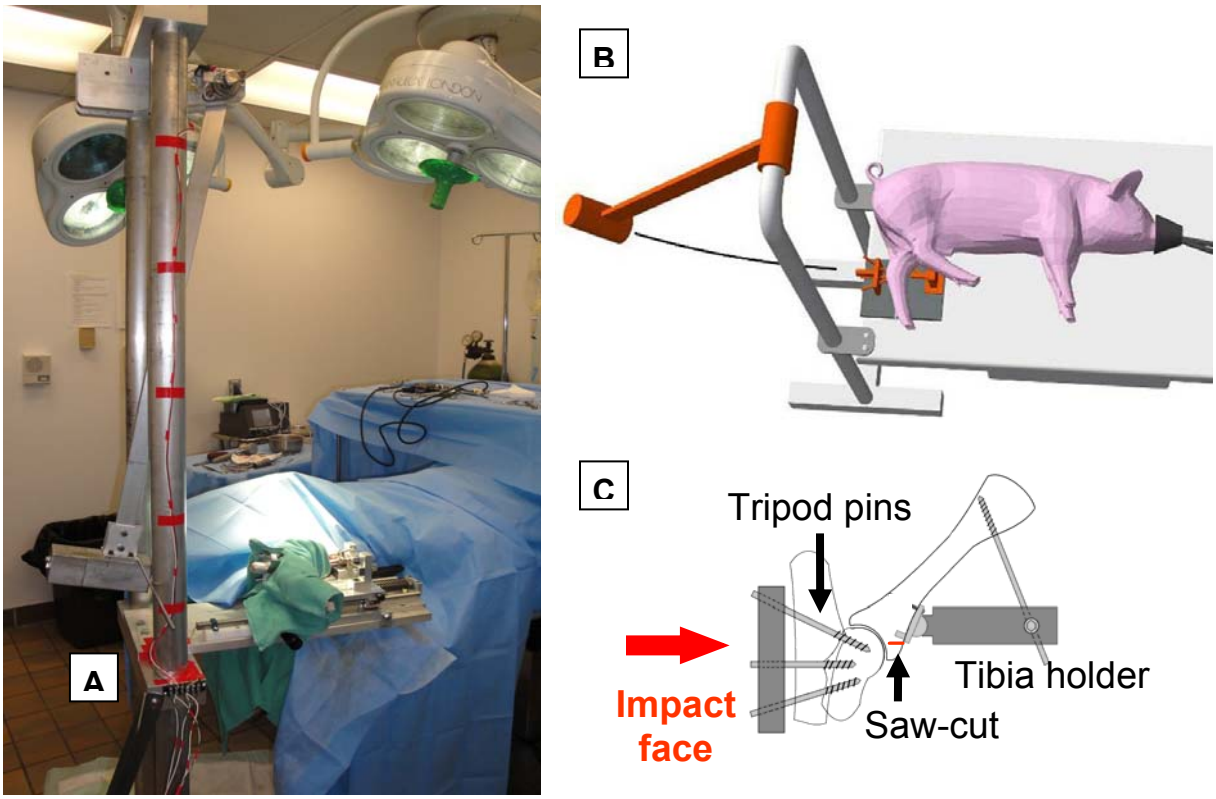

Figure 1. Surgical set-up of the custom pendulum-based impaction device (A), and schematics of fracture impaction (B) and the "offset" impaction technique.

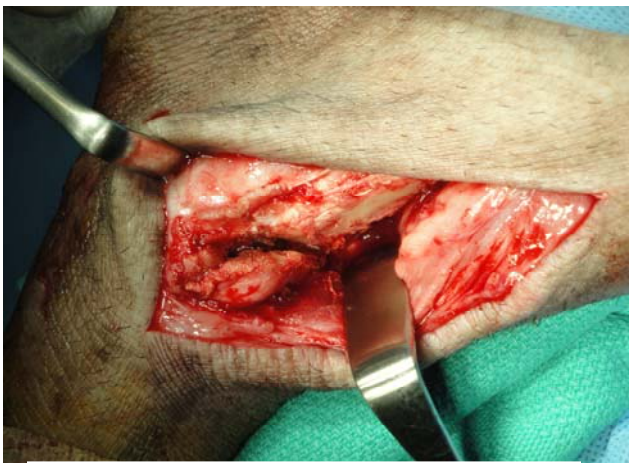

Figure 2. Intra-operative photograph of a representative case of experimental distal tibial intra-articular fracture.

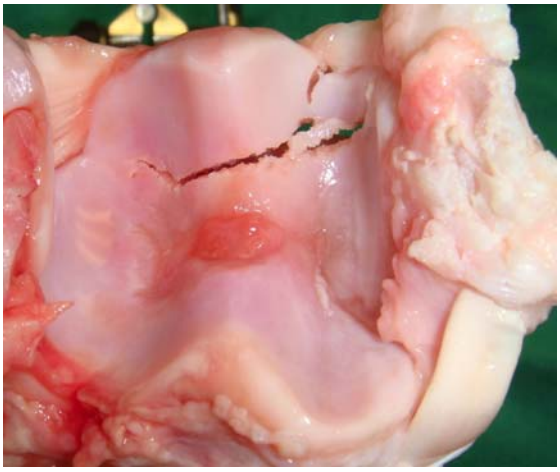

Figure 3. Articular surface view of a representative case of experimental distal tibial intra-articular fracture created in the cadaver pilot work.

2.1.b Post-Insult Management

The experimental fractures are surgically stabilized, either in an anatomically reduced position or in an intentionally displaced “2 mm step-off” position to replicate residual joint incongruity following mal-reduced fracture fixation. The internal fixation technique utilized (Figure 4) is very consistent with “standard-of-care” techniques for human clinical intraarticular fractures. The primary fixation implant employed throughout the three testing series is a clover-shaped locking plate designed for canine proximal tibial osteotomy (SYNTHES® Vet 2.7 mm TPLO plate, Synthes GmbH, Solothurn, Switzerland). This plate is placed on the anterior aspect of the distal tibial shaft (using three bi-cortical screws), so as to provide a “buttress” effect for the anterior malleolar fragment. Through the central hole of the clover-shaped head, one distal locking screw is placed for fragment stabilization. To provide additional rotational stability, one antero-medial “anti-rotation” screw (out side of the clover plate) is also placed. For step-off cases, an extra small T-plate is utilized to provide additional stability for the anti-rotation screw fixation. During the first week after surgery, supplemental external stabilization (a fiberglass cast) is used. Post-operatively, the animals are permitted unlimited activity under pen confinement.

Of the sixteen experimental fractures created to date, eight have been stabilized in an anatomically reduced position, while the other eight were in a “2 mm step-off” position. In the earlier two testing series (12 animals), we experienced three cases of post-operative complication. In one case, the distal screw was exposed at the articular surface (due to the small size of anterior malleolar fragment), and this case rapidly developed iatrogenic arthritis. We also have experienced two cases of post-operative fracture dislocation within 2 weeks of the index surgery. In these earlier series, regardless of reduction modality, we did not utilize the medial T-plate. To improve initial fixation stability for step-off reduction cases, we have modified the fixation techniques as noted above. An extra process to reconfirm distal screw positioning also has been added to reduce the potential for screw exposure. After these technical refinements, in the ongoing third testing series (including four step-off reduction cases), no such post-operative complications have been observed as of 8 weeks from the index surgery.

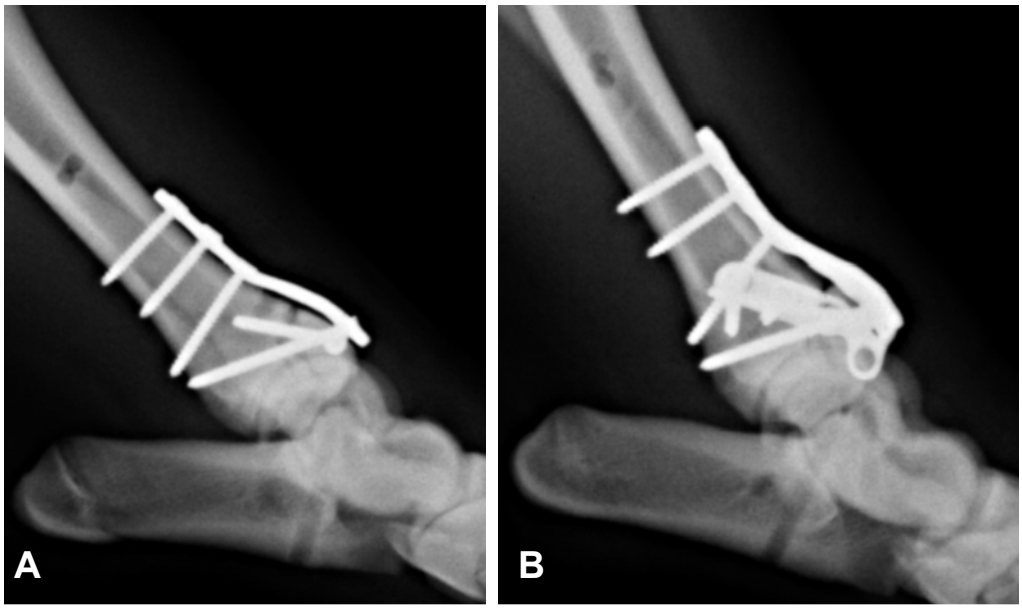

Figure 4. Representative cases of the latest fracture internal fixation techniques for anatomical reduction cases (A) and step-off reduction cases (B).

2.2 Natural Course of Experimental Fracture

2.2.a Radiographic Bone Healing

Fracture fixation stability and bone healing are radiographically followed at 3 days and at 1/2/4/8/12 weeks after index surgery.

As noted above, in the earlier two series, successful fracture creation and internal fixation were achieved in seven experimental joints (Figure 5). Of these, six experimental joints exhibited apparent radiographic bone healing in 12 weeks of fracture insult. One experimental joint in the first series exhibited signs of delayed union, specifically widening of the fracture gap (from week 2), which in turn resulted in decreasing density of the anterior malleolar fragment. (Note: When this experimental joint was dissected at 12 weeks post-surgery, stable bone healing was apparent in manual inspection.)

In the ongoing series, all of the six experimental joints exhibited stable fracture fixation as of the 8-week follow-up radiographs, and none of them exhibited signs of delayed union.

Figure 5. Lateral radiographs of the experimental joints 12 weeks after index surgery. (Note: the radiographs for #2, #3, and #4 were taken after implant removal.)

2.2.b Experimental Limb Usage

A pressure sensing walkway system (Tekscan Inc., North Boston, MA) is utilized for subjective evaluation of the side-to-side asymmetry of hind-leg usage during walking. Each animal is subjected to footprint contact stress measurement prior to the fracture insult (baseline), as well as at 1, 2, 4, 8, and 12 weeks after index surgery. Hind-leg usage asymmetry is then assessed in terms of the contribution of the experimental (left) hind-leg in vertical ground reactive force impulse.

The leg usage status in the seven fracture-healed animals (Figure 6) was characterized by significant load protection of the experimental leg (decreased contribution compared to the pre-operative baseline data) at 1 and 2 weeks after surgery ($p = 0.0002$ and < 0.0001, respectively). At these early post-operative points, the experimental leg's contribution was 30 to 40%. The contribution recovered to approximately 45% by 4 weeks.

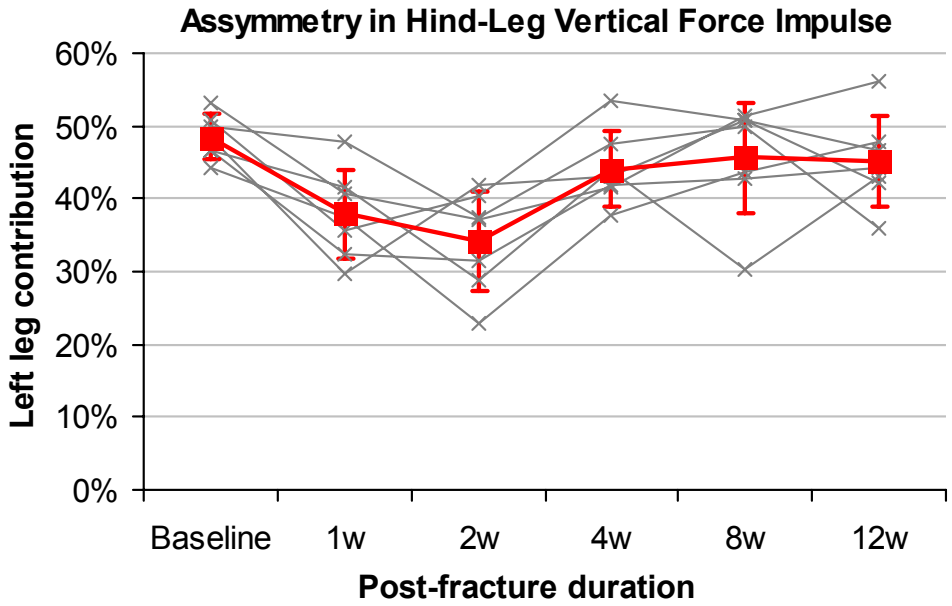

Figure 6. Gait analysis data in the seven fracture-healed animals. The values indicate relative contribution of the left (experimental) leg in hindfoot vertical force impulse. The X-plots are individual animal data. The filled squares and dispersion bars indicate means and standard deviations across animals.

2.2.c Evaluation of Joint Surface Incongruity

For every experimental joint, CT scans (0.3mm x 0.3mm x 1mm voxels) are acquired prior to fracture (baseline) and 12 weeks after index surgery. The outer cortex of the distal tibia is manually segmented using OsiriX (Pixmeo, Geneva, Switzerland), and smoothed into a continuous 3D surface using Geomagic Studio (Geomagic, Morrisville, NC, USA). Surfaces generated from post-surgery CT images are registered to their respective pre-surgery surfaces using an iterative closest-point technique in Geomagic Studio. The technique aligns portions of the tibia unaffected by fracture events (i.e., the shaft and the medial to posterior epiphyseal bone) while temporarily disregarding deviations resulting from the fracture (Figure 7). The distance between the registered surfaces perpendicular to the intact joint surface is then calculated, thus indicating changes in joint surface morphology resulting from the fracture insult, fixation, and healing process. The three fracture-healed experimental joints in the Series 1 have been analyzed to date.

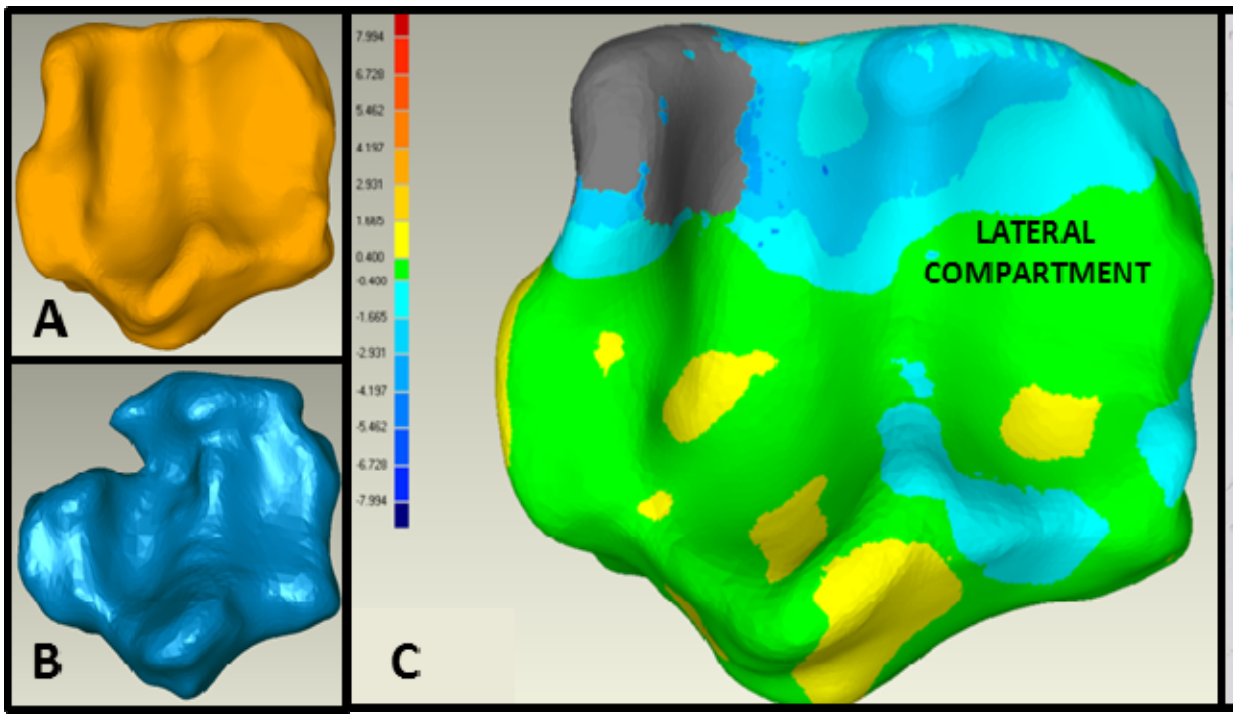

Figure 7. Representative case of joint surface incongruity analysis in a 2 mm step-off experimental joint (Case #4). Three-dimensional model of distal tibial articular surface pre-insult (A) and at 12 weeks after fracture (B). Using a combined computational registration technique, deviations in articular surface geometries (C) is analyzed. Green indicates minimal deviation, yellow indicates slightly elevated surface, and shades of blue indicate depression (i.e., step-off surface). Gray is outside the range of calculation (presumably indicating bone defect or decalcified bone in the vicinity of fracture line).

2.2.d Histological Outcomes

At the end of testing period (12 weeks after index surgery), the experimental joints are dissected and prepared for histological evaluation of articular cartilage condition. The specimens are processed following the OARSI guidelines[2], and histological sections are stained by Safranin O-Fast Green. The regions of interest are the medial and lateral tibial sagittal sections for both the tibial and talar surfaces.

Histological sections from the three fracture-healed joints tested in the first series (Figure 8) have been finished prepared to date. Of these three joints, cartilage degeneration was least in the anatomically reduced (Figure 8A). On the fracture-healed tibial surface, distinct proteoglycan (PG) depletion was observed only in the vicinity of the fracture line. Interestingly, the corresponding region on the opposing talar cartilage also exhibited PG depletion. In the step-off reduced joint (Figure 8A), the anterior malleolar step-off surface was covered by fibrous cartilage. Again, the talar cartilage exhibited PG depletion in the corresponding region. The union-delayed joint (Figure 8C) also exhibited distinctly greater PG depletion than the well-healed anatomically reduced joint (Figure 8A). Observations in these first three joints appear to be very consistent with our empirical knowledge in human clinical settings.

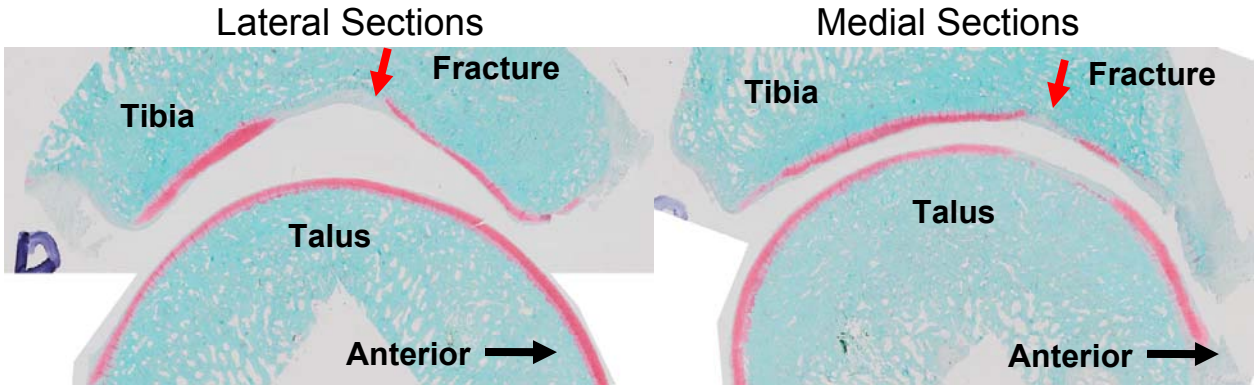

A: Anatomical reduction (well-healed)

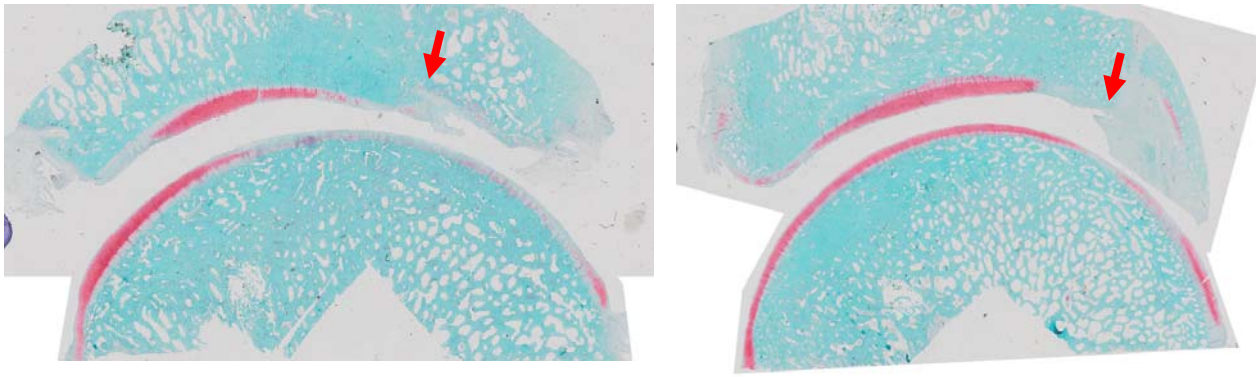

B: Step-off reduction (well-healed)

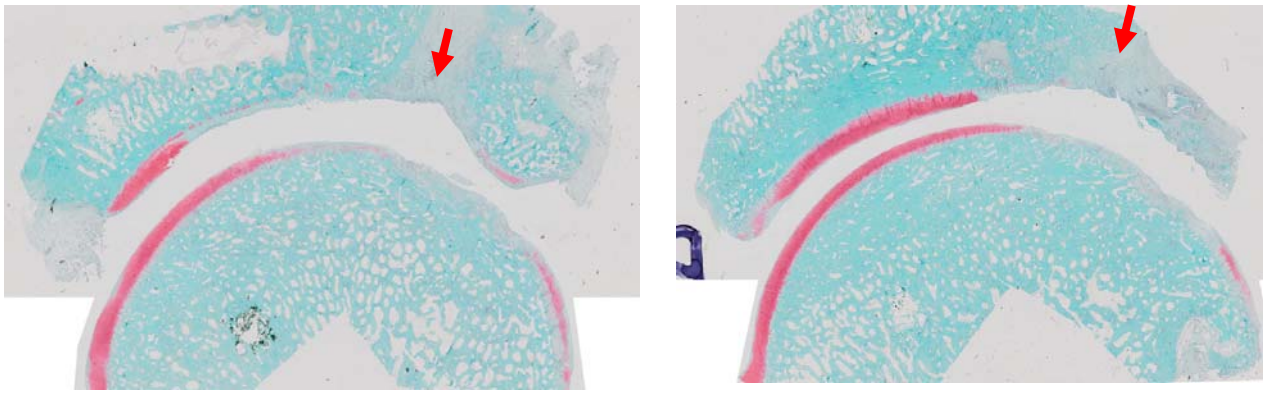

C: Delayed union (anatomical reduction)

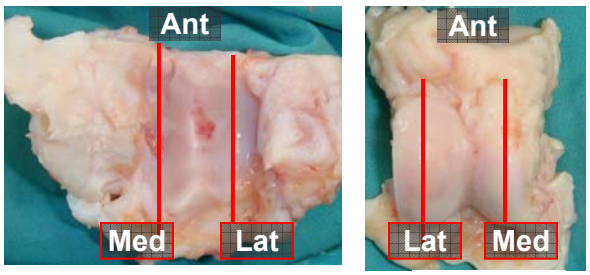

Tibia Talus

Figure 8. Sagittal histological sections (stained by SafraninO - Fast Green) from the first test series. (Note: These histological images are collages, in which the talar images have been manually apposed to show the relationship between opposing surfaces.) The location and orientation of the histological sections for the tibial and talar surfaces are illustrated on the left panels.

3. Key Research Accomplishments

- Refinement of the impaction insult protocol for improved reproducibility of fracture creation.
- Surgical and post-operative management protocols that permit replication of clinically realistic biological and biomechanical conditions in the fractured experimental joints.
- Gail analysis technique that enables quantitative evaluation of asymmetry in hind-limb usage, and confirmation of gradual recovery of experimental joint usage.
- CT-based image analysis technique that enables quantitative evaluation of joint incongruity in the fractured experimental joints.
- Confirmation of radiographic fracture healing in a time course very consistent with the post-injury time course of human clinical IAFs.
- Confirmation of cartilage histological findings consistent with human post-traumatic OA.

4. Reportable Outcomes

4.1. Peer-reviewed Papers

- Tochigi Y, Buckwalter JA, Martin JA, Hillis SL, Zhang P, Vaseenon T, Lehman AD, Brown TD. *Distribution and progression of chondrocyte damage in a whole-organ model of human intra-articular fracture.* J Bone Joint Surg Am. 2011 Mar;93(6):533-9.
- Tochigi, Y; Zhang, P; Rudert, MJ; Baer, TE; Martin, JA; Hillis, SL; Brown, TD. *A novel impaction technique for modeling intra-articular fracture in large animal joints. Osteoarthritis Cartilage* (in print).

4.2 Meeting Abstracts/Presentations

- Diestelmeier, BW; Rudert, MJ; Tochigi, Y; Baer, TE; Fredericks, DC; Brown, TD. *Quantification impaction system for a large animal survival model of intraarticular fracture.* 36th Annual Meeting of the American Society of Biomechanics, August 15–18, 2012, Gainesville, Florida. [Appendix 3]
- Tochigi, Y; Arunakul, M; Goetz, JE; Fredericks, DC; Martin, JA; Diestelmeier, BW.; Brown, TD; McKinley, TO. *Clinically relevant OA progression in a rabbit knee survival model of medial meniscus destabilization.* 2013 Annual Meeting of the Orthopaedic Research Society, January 26–29, 2013, San Antonio, Texas. (abstract submitted)
- Tochigi, Y; Diestelmeier, BW; Rudert, MJ; Baer, TE.; Fredericks, DC.; Arunakul, M; Brown, TD. *A clinically-realistic large animal survival model of human intra-articular fracture.* 2013 Annual Meeting of the Orthopaedic Research Society, January 26–29, 2013, San Antonio, Texas. (abstract submitted)
- Swanson, E; Goetz, JE; Tochigi Y. *Evaluation of articular surface geometry deviation and cartilage damage in a porcine model of intra-articular fracture.* 2013 Annual Meeting of the Orthopaedic Research Society, January 26–29, 2013, San Antonio, Texas. (abstract submitted)

4.3 Degrees Obtained

- *Design and application of an instrumented pendulum device for measuring energy absorption during fracture insult in large animal joints in vivo.* M.S. thesis, Bryce W.

Diestelmeier, Department of Biomedical Engineering, The University of Iowa, 2012.

4.4 Research Grants (funded)

- US Department of Defense (Department of Army) CDMRP-PRMRP
  Technology/Therapeutic Development Award W81XWH-11-1-0583
  Mitochondrial Based Treatments that Prevent Posttraumatic Osteoarthritis in a Translational Large Animal Intraarticular Fracture Survival Model
  (PI: Todd O. McKinley, MD)
- NIH/NIAM CORT Grant 5 P50 AR055533
  Innovations to Assess and Forestall Post-Traumatic Osteoarthritis
  (Program Director: Joseph A. Buckwalter, MD)
  Project-2: Establishing Treatments and Diagnostic Tools for Post-Traumatic OA In Vivo.
  (Project PI: Yuki Tochigi, MD, PhD)

5. Conclusion

As reported above, our PY-2 work has yielded a definitive protocol to create a large animal survival IAF model (Milestone #2 in the SOW) and a definitive protocol to document/analyze the natural course of fractured experimental joints in this model (Milestone #3).

In PY-3, documentation/analysis of the natural course data will be continued so as to achieve Milestone #4. Simultaneously, using the protocols established in the last two project years, the 7-day survival study to test the effect of a therapeutic treatment (Aim 3) will be pursued.

6. References

1. Diestelmeier, BW. 2012. Design and application of an instrumented pendulum device for measuring energy absorption during fracture insult in large animal joints *in vivo*. The University of Iowa, Iowa City.
2. Pritzker, KP, Gay, S, Jimenez, SA, et al. 2006. Osteoarthritis cartilage histopathology: grading and staging. Osteoarthritis Cartilage 14: 13-29.
3. Tochigi, Y, Zhang, P, Rudert, MJ, et al. (in print). A novel impaction technique to create experimental articular fractures in large animal joints. Osteoarthritis Cartilage. (Appendix)

A Novel Impaction Technique to Create Experimental Articular Fractures in Large Animal Joints

Manuscript prepared for *Osteoarthritis and Cartilage*

September 22, 2012

Authors:

Yuki Tochigi, MD, PhD
Department of Orthopaedics and Rehabilitation, University of Iowa
Email: yuki-tochigi@uiowa.edu

Peng Zhang, MD, PhD,
Department of Orthopaedics and Rehabilitation, University of Iowa, and Department of Orthopaedics, Affiliated Hospital of Shan Dong University of Traditional Chinese Medicine
Email: pengzhang.med@gmail.com

M. James Rudert, PhD
Department of Orthopaedics and Rehabilitation, University of Iowa
Email: jim-rudert@uiowa.edu

Thomas E. Baer, BA
Department of Orthopaedics and Rehabilitation, University of Iowa
Email: thomas-baer@uiowa.edu

James A. Martin, PhD
Department of Orthopaedics and Rehabilitation, University of Iowa
Email: james-martin@uiowa.edu

Stephen L. Hillis, PhD
Department of Biostatistics, University of Iowa, and Center for Research in the Implementation of Innovative Strategies in Practice (CRIISP), VA Iowa City Medical Center
Email: steve-hillis@uiowa.edu

Thomas D. Brown, PhD
Department of Orthopaedics and Rehabilitation, and Department of Biomedical Engineering, University of Iowa
Email: tom-brown@uiowa.edu

Correspondence to: Yuki Tochigi, MD, PhD
University of Iowa Orthopaedic Biomechanics Laboratory
2181 Westlawn
Iowa City, IA 52242-1100
Phone: (319) 335-7547
Fax: (319) 335-7530
Email: yuki-tochigi@uiowa.edu

Abstract

Objective: A novel impaction fracture insult technique, developed for modeling post-traumatic osteoarthritis in porcine hocks *in vivo*, was tested to determine the extent to which it could replicate the cell-level cartilage pathology in human clinical intra-articular fractures.

Design: Eight fresh porcine hocks (whole-joint specimens with fully viable chondrocytes) were subjected to fracture insult. From the fractured distal tibial surfaces, osteoarticular fragments were immediately sampled and cultured *in vitro* for 48 hours. These samples were analyzed for the distribution and progression of chondrocyte death, using the Live/Dead assay. Five control joints, in which "fractures" were simulated by means of surgical osteotomy, were also similarly analyzed.

Results: In the impaction-fractured joints, chondrocyte death was concentrated in regions adjacent to fracture lines (near-fracture regions), as evidenced by fractional cell death significantly higher ($p < 0.0001$) than in central non-fracture (control) regions. Although nominally similar spatial distribution patterns were identified in the osteotomized joints, fractional cell death in the near-osteotomy regions was nine-fold lower ($p < 0.0001$) than in the near-fracture regions. Cell death in the near-fracture regions increased monotonically during 48 hours after impaction, dominantly within 1 mm from the fracture lines.

Conclusion: The impaction-fractured joints exhibited chondrocyte death characteristics reasonably consistent with those in human intra-articular fractures, but were strikingly different from those in "fractures" simulated by surgical osteotomy. These observations support promise of this new impaction fracture technique as a mechanical insult modality to replicate the pathophysiology of human intra-articular fractures in large animal joints *in vivo*.

Keywords: intra-articular fracture, animal modeling, mechanical insult, cartilage injury, chondrocyte death

Running headline: Fracture Impaction for Animal Modeling

Introduction

Intra-articular fractures are a leading cause of post-traumatic osteoarthritis (OA).[1] Recently, the acute cell-level cartilage damage involved in intra-articular fractures has been receiving increasing attention.[2-8] Death or dysfunction of chondrocytes necessarily affects cartilage metabolism in injured joints, presumably triggering a pathological cascade that eventually leads to OA. Therapeutic treatments that amend this disease process (as adjuncts to current surgical treatment) hold potential to mitigate the risk of OA development following intra-articular fractures. Several types of biologic treatments have proven capable of preserving the viability and/or function of chondrocytes in cartilage explants after mechanical or biochemical insult.[3,9,11,14-16] However, progress in translation of these scientific developments into clinical practice has been limited by the lack of a large animal survival model that physiologically mimics human intra-articular fractures, and that is in a size range compatible with surgical procedures utilized in human clinical settings.

For an animal disease model to be scientifically valid, pathophysiological realism is crucial. In the case of intra-articular fracture, this is presumably achievable by fracturing animal joints using a mechanical insult modality that reasonably replicates the injury mechanism of human clinical intra-articular fractures. For this purpose, a new fracture insult technique is here reported, that replicates the typical mechanism of human distal tibial plafond (pilon) fractures. In this technique, the porcine hock joint (human ankle analogue) is subjected to an injurious transarticular compressive force pulse, causing impaction fracture.

The objective of the present study was to determine the extent to which this new insult modality was capable of replicating the pathophysiological reality of human intra-articular fractures. For this purpose, two hypotheses were tested. First, we tested whether experimental joints insulted using the new impaction fracture technique would exhibit cell-level cartilage damage consistent with that in human

intra-articular fractures.[2-4,7,9] Specifically, this involved cell-level cartilage damage in the fracture-insulted joints being characterized by chondrocyte death concentrated near fracture lines. Second, we tested whether fractional chondrocyte death in these fracture-insulted joints would be significantly higher than that in "fractures" simulated by means of surgical osteotomy, as often has been used experimentally.[10-12] In addition, the temporal and spatial progression of cell death was evaluated for intervals up to 48 hours post-impaction.

Methods

Thirteen fresh hock joints from agricultural pigs (age 9 to 12 months, weight 120 to 150 kilograms) were obtained from a local abattoir. These specimens, harvested from animal bodies chilled overnight after euthanasia (following the United States Department of Agriculture regulations), were insulted within 24 hours of animal death. Soft tissue surrounding the joint was removed, while leaving the joint capsule and major ligaments intact. Eight specimens were subjected to the impaction fracture insult, while the remaining five were subjected to surgical osteotomy (i.e., fracture simulation control).

For the impaction fracture insult, the joint was mounted in a custom bone anchorage system (Figure 1A). In this system, an aluminum impact interface was connected to the talus, using three external fixator pins (6-millimeter diameter, Orthofix Inc., Lewisville, Texas, USA) arrayed in a tripod configuration. Two of these tripod pins were inserted directly into the talus, from inferomedially, toward the talar body. The third pin was inserted from the calcaneus to the talus, though the talocalcaneal joint. The tibia was restrained by a leg holder device, which consisted of a distal tibial plate and a solid rod. A ball-in-socket joint between the plate and the rod provided rotational adjustability, allowing the joint to be aligned appropriately relative to the impact force direction. This tibial plate was secured to the anterior distal tibial surface by two pegs on the plate, and by a cortical screw. An external fixator pin connected the rod to the proximal tibia, in order to maintain predetermined inclination of the tibial shaft

(approximately 45 degrees). This tibial inclination created an "offset" condition, by means of which a force pulse applied to the joint caused sudden elevation of vertical shear stresses in the anterior tibial juxtaarticular bone. A stress-rising sawcut was used to guide the location and orientation of fracture, to create fractures morphologically similar to human ankle anterior malleolar fractures. This cut was made on the anterior distal tibial cortex, 2-3 millimeters distal to the distal tibia plate, using a bone oscillator (HALL® oscillator, ConMed Corp., Largo, Florida, USA), typically stopping 5-7 millimeters short of the undersurface of the subchondral plate.

Thus anchored, the specimen was then mounted in a custom drop-tower device (Figure 1B), with the tibial side down, and with the distal impact face carefully aligned with the axis of mass fall. The tibial potting block was secured to a massive base plate. The distal impact face was lightly held (using masking tape) as horizontal as possible. A 6.55-kilogram mass was then dropped from 47-centimeter height, delivering approximately 30 joules of kinetic energy to the specimen. (Note: In pilot work, impaction insult in a no-stress-riser condition at 80J of energy delivery resulted in morphologically inconsistent distal tibial fractures, including highly comminuted fractures inadequate for survival animal modeling.) In the five control specimens, simulated "fractures" at the distal tibia were created, morphologically similar to those from the drop-tower impactions. In these control specimens, anterior tibial sawcuts were similarly made, but the simulated "fractures" were finished using a surgical osteotome, instead of by a falling mass.

Immediately after fracture creation, the joints were disarticulated, and the distal tibial articular surfaces were digitally photographed to record the fracture morphology. Next, using sterile technique, major osteoarticular fragments were sampled for chondrocyte death measurement. Due to the complicated geometry of the porcine distal tibial articular surface, to facilitate mircoscopy of the cartilage surface, large osteoarticular fragments were dissected into small pieces, with juxta-articular

bone being trimmed away, leaving approximately a five-millimeter thickness of cancellous bone beneath the cartilage layer. From each joint, three to five osteoarticular fragments were sampled, with a typical volume per specimen of approximately 1 cubiccentimeter. Each osteoarticular fragment was then secured to a specimen holder (Figure 2A and B), such that the articular surface near the fracture edge was held nearly horizontal, by potting in a non-exothermic biocompatible polymer (Polycaprolactone, Sigma-Aldrich, Inc., St. Louis, Missouri, USA). The potted specimen was then immersed in culture medium (approximately 80 mL per specimen), comprised of 45% Ham's F-12 Nutrient Mixture, 45% high glucose Dulbecco's Modified Eagle Medium, and 10% fetal bovine serum (all from Invitrogen Co., Carlsbad, California, USA), with a 1% anti-bacterial/-fungal mixture of pencicillin-streptomycin (Invitrogen) and amphotericin B (Thermo Scientific HyClone, Logan, Utah, USA), in an incubator maintained at 37°C under 5% CO_2.

After 48 hours of culture, chondrocyte death in these osteoarticular fragments was assessed using calcein AM for labeling live cells and ethidium homodimer-2 for labeling dead cells (again, both from Invitrogen Co.). Prior to analysis, the fragments were soaked in culture medium with these fluorescent stains (at a concentration of 1.0 micromolar each) for approximately one hour at 37°C. For each joint, scans of 540 x 540 micron square fields were executed at several sites adjacent to the primary fracture (or osteotomy) line (designated as the near-edge region), as well as at several sites centrally away from fragment edges in non-fracture areas (designated as the central region). For these central region scans, any sites with macroscopically identifiable structural damage (e.g., visible superficial cracks) were avoided. For every near-edge or central site, cartilage in the superficial zone (i.e., from the articular surface to a depth of typically 100 to 150 microns) was scanned at 20-micron intervals, using a confocal microscopy system (MRC-1024, Bio-Rad Laboratories, Hercules, California, USA). During scanning (which required 1 to 2 hours), the specimens were kept immersed in the regular medium at room temperature.

Of the eight impaction-fractured joints, three were scanned at multiple time points. From each of these three joints, three osteoarticular fragments were selected that included a relatively uniform primary fracture line. At the initial scanning time point (within two hours post-impact), for each fragment, two neighboring sites along the primary fracture line (Figure 2C) were selected, separated by 1 millimeter. For all of these paired fracture-edge sites, three contiguous 540 x 540 micron fields (one including the fracture line, along with the two next-centrally-adjacent image fields) were scanned. Typically, this allowed scanning out to 1.4 mm away from the fracture line. For each near-fracture site, two central region sites at least 3 mm away from the fracture line were also scanned. Of these two groups of scan sites established for each fragment, one was subjected to follow-up scanning at 6 and 12 hours post-fracture, and the other at 24 and 48 hours post-fracture. The x-y coordinate information at the initial scanning was recorded. Based on this coordinate information, scans at the later time points were repeated at the identical sites, using a custom-built programmable microscope x-y axis stage driver (positioning reproducibility < 25 microns). After each scanning session, the specimens were washed with Hanks balanced salt solution (#14170, Gibco-Invitrogen, Grand Island, New York, USA), containing 1% of the above-described anti-bacterial/-fungal mixture, after which they were placed into fresh culture media.

The scanned images were analyzed using ImageJ software (National Institute of Health, Bethesda, Maryland, USA). Image data for each site/time point consisted of two sets of multi-slice images, one for live cells labeled by green fluorescence, and the other for dead cells labeled by red fluorescence. The images, originally in gray scale, were converted to a binary format, allowing fluorescent-labeled cells to be counted using the software's particle analysis function. For every image set for live cells, the image intensity threshold for the binary conversion was adjusted such that all plausibly labeled cells were counted, and such that the same cells were not counted over neighboring multiple slices. The identical binary conversion threshold was utilized for cell counting for the

corresponding dead-cell image set. The minimum particle size thresholds for automated cell counting were 50 and 20 square-microns for live and dead cells, respectively. Live and dead cells were counted separately, and the fraction of dead cells among total cells (fractional cell death) in the region of interest was computed. Confocal images from multiple-time-point scans in near-edge regions, consisting of three contiguous scan fields, were parsed into seven zones in 0.2-mm intervals, and fractional cell death was computed separately for each zone (Figure 2D).

Differences in fractional cell death between the near-edge and central regions were analyzed using a logistic regression model with specimen random effects (also known as a hierarchical generalized linear model or a generalized linear model with random effects), using SAS® (Ver. 9.1.3, SAS Institute Inc., Cary, North Carolina, USA). Specifically, the fractional cell death data were treated as "pseudo-binomial" variables, i.e., the relationship of the mean and variance was assumed to be the same as for a binomial-variable proportion computed from independent trials (Appendix). Inclusion of the random effects accounted for within-specimen correlation, thus allowing conclusions to be generalized to the population of specimens from which the samples were considered representative, rather than being limited only to the specific specimens evaluated. Thus, the model accounted for the dependence of the variance of outputs on the true fractional cell death and on the number of cells, while also accounting for variability in the fractional cell death across specimens. There were four comparisons of interest; using a Bonferroni correction for multiple tests to limit the overall type I error to 0.05, these tests were considered conclusive if $p < 0.05 / 4 = 0.0125$. Mean values, 95% confidence intervals (CIs), and inter-quartile ranges (IQRs) were reported. For the time-wise analysis, given the small number of specimens (n =3), it was not feasible to use the above specimen-random-effects approach for detecting difference in the time-dependency of cell death between near-edge versus central (control) regions at any given time. Instead, six comparisons were made for each observation time, using two-sample *t*-tests. These time-wise comparisons were considered conclusive if $p < 0.05 / 6 = 0.0083$.

Results

At gross morphological inspection, all eight impacted joints were found to have a distal tibial fracture, with the primary fracture line running medially-laterally, typically in the anterior one-third of the distal tibial surface (Figure 3A). In these impaction-fractured joints, fractional cell death at 48 hours post-fracture was measured at 43 near-edge and 72 central sites (total counts across the eight joints). Time-wise changes in cell death were assessed at 9 near-edge and 18 central sites across three of the eight joints. Simulated "fractures" in the five osteotomized joints (Figure 3B) also exhibited similar gross morphological characteristics. Cell death in these osteotomized joints was assessed at 36 near-edge and 58 central sites.

In the 48-hour scan data for the impaction-fractured joints (Figures 4 and 5), the local fractional cell death ranged from 0.6 to 97.1% (IQR: 17.8 – 46.7) in near-edge regions (typically up to 0.3-0.4 millimeters away from a fracture line), and from 0.0 to 26.0% (IQR: 0.5 – 5.4) in central regions. The death fraction in near-edge regions (38.1%, CI: 25.7 – 52.2) was significantly higher ($p < 0.0001$) than that in central regions (4.6%, CI: 2.6 – 7.9). In the osteotomized specimens, death fraction ranged from 0.0% to 18.7% (IQR: 1.1 – 9.9%) in near-edge regions and from 0.0 to 15.9% (IQR: 0.1 – 1.4%) in central regions. The death fraction in near-edge regions (4.3%, CI: 2.1 – 8.6) was again significantly higher ($p < 0.0001$) than that in central regions (1.0%, CI: 0.5 – 2.0). When data were compared regarding the two insult modalities, for both near-edge and central regions, the death fraction in the impaction-fractured specimens was significantly higher (near-edge: $p < 0.0001$; central: $p = 0.0009$) than in the osteotomized specimens.

Regarding time-wise analysis (Figure 6), at the initial scanning time (within 2 hours of fracture), fractional cell death was comparable between near-edge regions (in this dataset, up to 1.4 millimeters away from a fracture line) and central regions, in both of the 6-12- and 24-48-hour datasets ($p = 0.56$ and 0.43, respectively). In both datasets, as cell death progressed with time dominantly in cartilage adjacent to the fracture lines, the difference attained statistical significance at 12 hours ($p < 0.001$), and remained so at 24 and 48 hours ($p = 0.0002$ and < 0.0001, respectively). When distributions of fractional cell death across the seven 0.2 millimeter-wide zones adjacent to the fracture lines were plotted for individual specimen/site combinations (Figure 7), distinctly high levels of chondrocyte death (indicated by fractional cell death exceeding the mean plus two standard deviations of the control central-region data) were typically identified within 1.0 mm of the fracture lines.

Discussion

The present study tested a novel mechanical insult modality suitable for modeling human clinical intra-articular fractures in large animal joints (here, porcine hocks) *in vivo*. This modality, designated as the "offset" impaction technique, was evaluated in a bench-top setting using fresh porcine hock specimens with initially full chondrocyte viability. Osteoarticular samples harvested from these joints were cultured *in vitro* and then subjected to cell death measurement. This *ex vivo* setting of course did not incorporate any effects from injury-associated biological responses, such as intra-articular bleeding and/or synovial inflammation. While this was a limitation in terms of injury realism, the lack of these extrinsic biological influences held the advantage of allowing study of the isolated effects of mechanical insult to articular cartilage. In this culture setting, exposed cancellous bone might have released molecules potentially injurious to cartilage, but any such effects would have been consistent across sites, specimens, and experimental groups. It should be noted that the drop-tower impaction system utilized in the present study was adopted for experimental convenience, but was not suitable for fracture insult to animal joints *in vivo*. Producing similar insults in survival animal surgery requires positioning flexibility

for attachment to the joint of interest, while permitting the animal's body to be held in a position appropriate for anesthesia and surgical management. These latter requirements are satisfied by use of a pendulum-based impaction system (Figure 8A), which consistently produces similarly well-controlled fracture patterns in porcine hocks *in vivo* (Figure 8B).

Cell-level acute cartilage damage in the impaction-fractured joints was characterized by chondrocyte death being concentrated along fracture lines. This spatial distribution pattern is analogous to that observed in small (surgical discard) osteoarticular fragments from clinical fracture cases,[2-4] as well to as that in previous whole-joint quasi-*in-vivo* models that utilized an insult modality closely replicating the injury mechanisms in human clinical cases to create "true" intra-articular fractures in the human ankle[7] or the porcine stifle.[9] The fractional cell death in cartilage adjacent to fracture lines in the impaction-fractured joints (mean 38.1%, CI: 25.7 – 52.2) is very consistent with that observed in true human ankle fractures at the same time-point (25.9%, CI: 18.7 – 33.1) in the quasi-*in-vivo* study.[7] The present insult protocol included placement of a stress riser to guide the location and orientation of fracture. While this stress riser was necessary for reproducible fracture creation (both morphologically and severity-wise), use of the stress riser reduced the magnitude of energy delivery otherwise needed for fracture creation, less than 40% of the magnitude needed in a no-stress-riser condition in pilot work (i.e, 30 vs. 80J; unpublished data). Due to lack of ability to reproducibly create such no-stress-riser fractures, the effects of this energy reduction on cell death characteristics could not be studied. However, given the observations noted above, regardless of the reduced energy delivery, the offset impaction technique proved capable of introducing experimental articular fractures in the porcine hock that share pathophysiological characteristics with human clinical intra-articular fractures.

The "fractures" simulated by surgical osteotomy also exhibited cell death preferentially concentrated in regions adjacent to the "fracture" lines. However, the fractional cell death in these

regions was much smaller (~ one-ninth) than that observed in corresponding regions in the impaction-fractured porcine joints, or in the above-mentioned human ankle quasi-*in-vivo* model.[7] This striking difference suggests that the physical stress to which chondrocytes were exposed was very different between these two insult modalities. One possible explanation for this difference is the extreme instantaneous cartilage deformation during a fracture event. During impaction, articular cartilage in the contact area would be highly compressed up until the instant when the cartilage-bone complex fractures, thus building up extremely high cartilage internal pressure. Once the articular surface fractures, however, cartilage along fracture lines would abruptly lose buttressing effects from the adjunct cartilage, resulting high stress gradients, leading to abrupt cartilage deformation that would damage chondrocytes.

The time-wise analysis characterized the process of cartilage damage progression in fractured joints. Although fractional cell death was variable across specimens/sites, relatively linear increase of cell death with time was exhibited in regions adjacent to fracture lines. This observation suggests involvement of active factors in contributing to the relatively broad (up to 1 mm) bands of cell death along fracture lines. The cause of this cell death progression might be from delayed apoptosis (resulting directly from physical stress at the instant of fracture), from the cytotoxic effect of biological mediators released from damaged chondrocytes and/or from the disrupted extracellular matrix,[13-15] or both. Although the mechanisms of the delayed cell death were not explored in the present study, at the time immediately after injury, some of the dying cells might have been potentially rescuable. Assuming that the process of disease progression is similar in clinical intra-articular fractures, experimental articular fractures created in large animal *in vivo* using the present offset impaction technique would permit piloting new treatment strategies (such as cytoprotective intervention[16-21]) to mitigate additional cartilage damage occurring during this period. Given the relatively monotonic increase of cell death with time, the best treatment outcome would be expected if such intervention is applied at the earliest possible time point.

In the present study, the pathology of fracture-associated cartilage injury was assessed in terms of chondrocyte death in the superficial zone, characteristics of which in intra-articular fractures have been well documented in the literature.[2,7,9] Cell viability was assessed only by a single technique, the Live/Dead assay, which did not discriminate the mechanisms of cell death. A major advantage of focusing only on cell death in the superficial zone was that repetitive measurements at the same sites enabled longitudinal observations of changes in the cell death distribution. Unfortunately, as a trade-off, the associated restriction in specimen positioning (due to specimen potting) did not permit assessing cell death on cross sections, and pathological details of fracture-associated cartilage damage in deeper zones could not be explored. In a previous study, Backus et al.[9] assessed details of the cross-sectional distribution of cell death in porcine stifle intra-articular fractures created (*ex vivo*) by means of an impaction insult to whole-joint constructs. They found that cell death in regions immediately adjacent to fracture lines (within 100 microns) was distributed across the entire thickness, whereas that in the next-neighboring regions (100-200 microns) was concentrated in the superficial zone. Given the similarities of the fracture insult methodology, similar cross-sectional fractional death distributions presumably occurred in the present study. Additional key observations by Backus et al.[9] were that central non-fracture regions on fractured surfaces exhibited a relatively small fraction of cell death, limited to the superficial zone, and that similar cell death characteristics were found in joints after an equivalent magnitude of non-fracturing impaction. These previous observations, along with the relatively small fraction of superficial cell death in central non-fracture regions in the present study, suggest that cartilage-on-cartilage blunt impaction is not a major cause of the cell-level cartilage injury seen for intra-articular fractures.

In conclusion, the offset impaction technique documented in the present study was capable of reproducibly creating morphologically well-controlled experimental articular fractures in porcine hocks. Cartilage damage resulting from fracture-line-controlled impacts was not noticeably different from that

in the existing knowledge base of non-fracture-line-controlled impacts (e.g., clinical intra-articular fractures), but strikingly different from that associated with surgical osteotomy. Given that the offset impaction technique is applicable to fracture insult *in vivo*, this novel insult modality holds promise for replicating the pathophysiology of human intra-articular fractures in a large animal survival model.

Acknowledgement

This research was supported by the University of Iowa Biological Sciences Funding Program, by an Orthopaedic Trauma Association Research Grant, by NIH CORT Grant P50 AR055533, and by US Department of Defense CDMRP-PRORP Technology Development Award W81XWH-10-1-0864.

Author contributions

YT, MJR, and TEB contributed to the conception, design, and fabrication of the impaction fracture system. YT, PZ, and JAM contributed to the validation experiment and to interpretation of the data. YT and SLH designed and conducted statistical analysis. TDB oversaw the overall study and contributed to manuscript preparation by providing critical suggestions, particularly for scientific content. All authors gave final approval of the manuscript version submitted.

Conflict of interest

None.

Role of the funding source

The sponsors listed above were the only funding sources for this research project. None of the above-noted financial sponsors had any involvement in the process of data analysis or manuscript preparation.

Appendix

Differences in fractional cell death between the near-edge and central regions were studied using a logistic regression model, with specimen-random effects. Inclusion of the random effects accounts for within-specimen correlation, thus allowing conclusions to be generalized to the overall population of specimens of which our sample can be considered representative, rather than being limited only to the specimens used in this particular experiment. Let Y_{ijkl} denote the fraction of dead cells observed at site *l* in specimen *i* at location level *j* (*j* = 1 if near-edge, 2 if central) subjected to insult type *k* (*k* = 1 if impaction fracture, 2 if osteotomy). For a given specimen, insult type, and location level, the Y_{ijkl} are assumed to be independent across sites with mean p_{ijk} and variance $p_{ijk}\left\lfloor 1-p_{ijk}\right\rfloor / n_{ijkl}$, where n_{ijkl} is the total number of cells corresponding to Y_{ijkl}. Thus we are treating Y_{ijkl} as a "pseudo-binomial" variable, in the sense that we assume the relationship of its mean (i.e., probability of cell death) and variance is similar to that for a binomially-variable proportion. Our motivation for this approach is as follows: Although the fractional deaths are not true binomial variables (because they do not represent the ratio of a count over a total number of independent Bernoulli trials), they are similarly computed and bounded (by 0 and 1). See McCullagh and Nelder[22] for a discussion of this approach.

The p_{ijk} are modeled by the equation

$$\text{logit}\left(p_{ijk}\right)=\mu_{jk}+s_{i(k)};i=1,\ldots,n_k;\ j=1,2;k=1,2$$

where $\text{logit}\left(p_{jk}\right)=\log\left\lfloor p_{jk}/\left(1-p_{jk}\right)\right\rfloor$, the μ_{jk} are fixed effects, $n_1=8$ and $n_2=5$ are the number of specimens subjected to impaction fracture and osteotomy, respectively, and the $s_{i(k)}$ are random effects (corresponding to specimens nested within insult type) that are independently and normally distributed with zero mean. This model allows the probability of cell death to depend on region (near-edge vs.

central) and to vary across specimens, with the population probability of death for location *j* and impact level *k* given by $\exp(\mu_{jk}) / \lfloor 1 + \exp(\mu_{jk}) \rfloor$.

In summary, this model accounts for the dependence of the variance of the fractional cell death on the true proportions and the number of cells, and accounts for variability in the rates across specimens. Other names for this model are hierarchical generalized linear model and generalized linear model with random effects; see Raudenbush and Bryk[23] for a further discussion of such models. We fitted this model using PROC GLIMMIX in SAS® (Ver. 9.1.3, SAS Institute Inc., Cary, North Carolina, USA), with a logit link function and a binomial variance function. Pearson residual plots supported the use of the binomial variance function.

References

1. Brown TD, Johnston RC, Saltzman CL, Marsh JL, Buckwalter JA. Posttraumatic osteoarthritis: a first estimate of incidence, prevalence, and burden of disease. J Orthop Trauma 2006;20:739-44.
2. Hembree WC, Ward BD, Furman BD, Zura RD, Nichols LA, Guilak F, et al. Viability and apoptosis of human chondrocytes in osteochondral fragments following joint trauma. J Bone Joint Surg Br 2007;89:1388-95.
3. Kim HT, Lo MY, Pillarisetty R. Chondrocyte apoptosis following intraarticular fracture in humans. Osteoarthritis Cartilage 2002;10:747-9.
4. Murray MM, Zurakowski D, Vrahas MS. The death of articular chondrocytes after intra-articular fracture in humans. J Trauma 2004;56:128-31.
5. Furman BD, Olson SA, Guilak F. The development of posttraumatic arthritis after articular fracture. J Orthop Trauma 2006;20:719-25.

6. Furman BD, Strand J, Hembree WC, Ward BD, Guilak F, Olson SA. Joint degeneration following closed intraarticular fracture in the mouse knee: a model of posttraumatic arthritis. J Orthop Res 2007;25:578-92.
7. Tochigi Y, Buckwalter JA, Martin JA, Hillis SL, Zhang P, Vaseenon T, et al. Distribution and progression of chondrocyte damage in a whole-organ model of human ankle intra-articular fracture. J Bone Joint Surg Am 2011;93:533-9.
8. McKinley TO, Borrelli J, Jr., D'Lima DD, Furman BD, Giannoudis PV. Basic science of intra-articular fractures and posttraumatic osteoarthritis. J Orthop Trauma 2010;24:567-70.
9. Backus JD, Furman BD, Swimmer T, Kent CL, McNulty AL, Defrate LE, et al. Cartilage viability and catabolism in the intact porcine knee following transarticular impact loading with and without articular fracture. J Orthop Res 2011;29:501-10.
10. Lefkoe TP, Trafton PG, Ehrlich MG, Walsh WR, Dennehy DT, Barrach HJ, et al. An experimental model of femoral condylar defect leading to osteoarthrosis. J Orthop Trauma 1993;7:458-67.
11. Convery FR, Akeson WH, Keown GH. The repair of large osteochondral defects. An experimental study in horses. Clin Orthop Relat Res 1972;82:253-62.
12. Vaseenon T, Tochigi Y, Heiner AD, Goetz JE, Baer TE, Fredericks DC, et al. Organ-level histological and biomechanical responses from localized osteoarticular injury in the rabbit knee. J Orthop Res 2011;29:340-6.
13. Clements KM, Burton-Wurster N, Lust G. The spread of cell death from impact damaged cartilage: lack of evidence for the role of nitric oxide and caspases. Osteoarthritis Cartilage 2004;12:577-85.
14. Levin A, Burton-Wurster N, Chen CT, Lust G. Intercellular signaling as a cause of cell death in cyclically impacted cartilage explants. Osteoarthritis Cartilage 2001;9:702-11.
15. Goodwin W, McCabe D, Sauter E, Reese E, Walter M, Buckwalter JA, et al. Rotenone prevents impact-induced chondrocyte death. J Orthop Res 2010;28:1057-63.

16. Ramakrishnan P, Hecht BA, Pedersen DR, Lavery MR, Maynard J, Buckwalter JA, et al. Oxidant conditioning protects cartilage from mechanically induced damage. J Orthop Res 2010;28:914-20.
17. Martin JA, McCabe D, Walter M, Buckwalter JA, McKinley TO. N-acetylcysteine inhibits post-impact chondrocyte death in osteochondral explants. J Bone Joint Surg Am 2009;91:1890-7.
18. D'Lima D, Hermida J, Hashimoto S, Colwell C, Lotz M. Caspase inhibitors reduce severity of cartilage lesions in experimental osteoarthritis. Arthritis Rheum 2006;54:1814-21.
19. Phillips DM, Haut RC. The use of a non-ionic surfactant (P188) to save chondrocytes from necrosis following impact loading of chondral explants. J Orthop Res 2004;22:1135-42.
20. Rundell SA, Baars DC, Phillips DM, Haut RC. The limitation of acute necrosis in retro-patellar cartilage after a severe blunt impact to the in vivo rabbit patello-femoral joint. J Orthop Res 2005;23:1363-9.
21. Kurz B, Lemke A, Kehn M, Domm C, Patwari P, Frank EH, et al. Influence of tissue maturation and antioxidants on the apoptotic response of articular cartilage after injurious compression. Arthritis Rheum 2004;50:123-30.
22. McCullagh P, Nelder JA. Generalized Linear Models. Chapman and Hall, London, UK 1989:328-32.
23. Raudenbush SW, Bryk AS. Hierarchical linear models: applications and data analysis methods. Sage Publications, Thousand Oaks, California, USA 2002.

Figure legends

Figure 1. (A) Schematic of the tripod bone anchorage system for the "offset" fracture impaction technique. **(B)** A porcine hock specimen mounted using the anchorage system, in the custom drop-tower system for delivering a fracture impaction force pulse.

Figure 2. Chondrocyte viability analysis. **(A)** Specimen sampling from the fractured distal tibial surface. **(B)** An osteoarticular sample mounted on the specimen holder. **(C)** Scanning site selection for the time course analysis. **(D)** Live/dead cell counting in the superficial zone (within 100 to 150 microns of the articular surface), in 0.2-millimeter intervals in a region neighboring a fracture line.

Figure 3. Examples of **(A)** experimental porcine distal tibial fractures created using the offset impaction technique and **(B)** "fractures" conventionally simulated by surgical osteotomy.

Figure 4. Confocal microscope images of superficial chondrocyte viability in representative regions adjacent to a fracture line (A) or an osteotomy line (B), at 48 hours post-insult. Live cells are labeled by green fluorescence, while dead cells are labeled red.

Figure 5. Chondrocyte viability in the superficial zone, at 48 hours after impaction fracture vs. osteotomy, in near-edge regions (typically up to 0.3-0.4 mm away from a fracture/osteotomy line) and in central (control) regions. The scatter plots indicate fractional cell death for each specimen/site combination, from the eight impaction-fractured (Fx) and five osteotomized (Os) specimens. The filled squares/diamonds and dispersion bars indicate (estimated) means calculated in the logistic regression analysis, and 95% confidential intervals, respectively.

Figure 6. Time course changes of fractional cell death in the superficial zone, in the 6-12- and 24-48-hour datasets. The filled squares indicate the means of fractional cell death in seven 0.2 mm-wide zones in near-edge regions, while the filled diamonds are for those in central regions, both across nine observation sites in three joints The dispersion bars indicate 95% confidential intervals. Near-edge fractional death values for each specimen/site combination (the means across seven 0.2 mm-wide zones) are also individually plotted.

Figure 7. Spatial distribution of fractional cell death in the superficial zone, at 12 or 48 hours post-fracture. The filled squares and dispersion bars indicate the mean values and 95% confidential intervals of fractional cell death measured separately for seven 0.2 mm-wide zones. Data from each specimen/site combination are also individually plotted. The red solid lines indicate the upper limit of normative range (mean plus two standard deviations) of fractional death in central regions, at each observation time.

Figure 8. (A) Schematic diagram of the pendulum impact device for delivering an impaction force pulse in survival animal surgeries. (B) Lateral radiographs of porcine hock experimental fractures created *in vivo*, using the offset impaction technique, in a pilot series (n = 4) of an ongoing survival study.

Figure 1
Click here to download Figure: Figure 1R.pdf

Figure 1

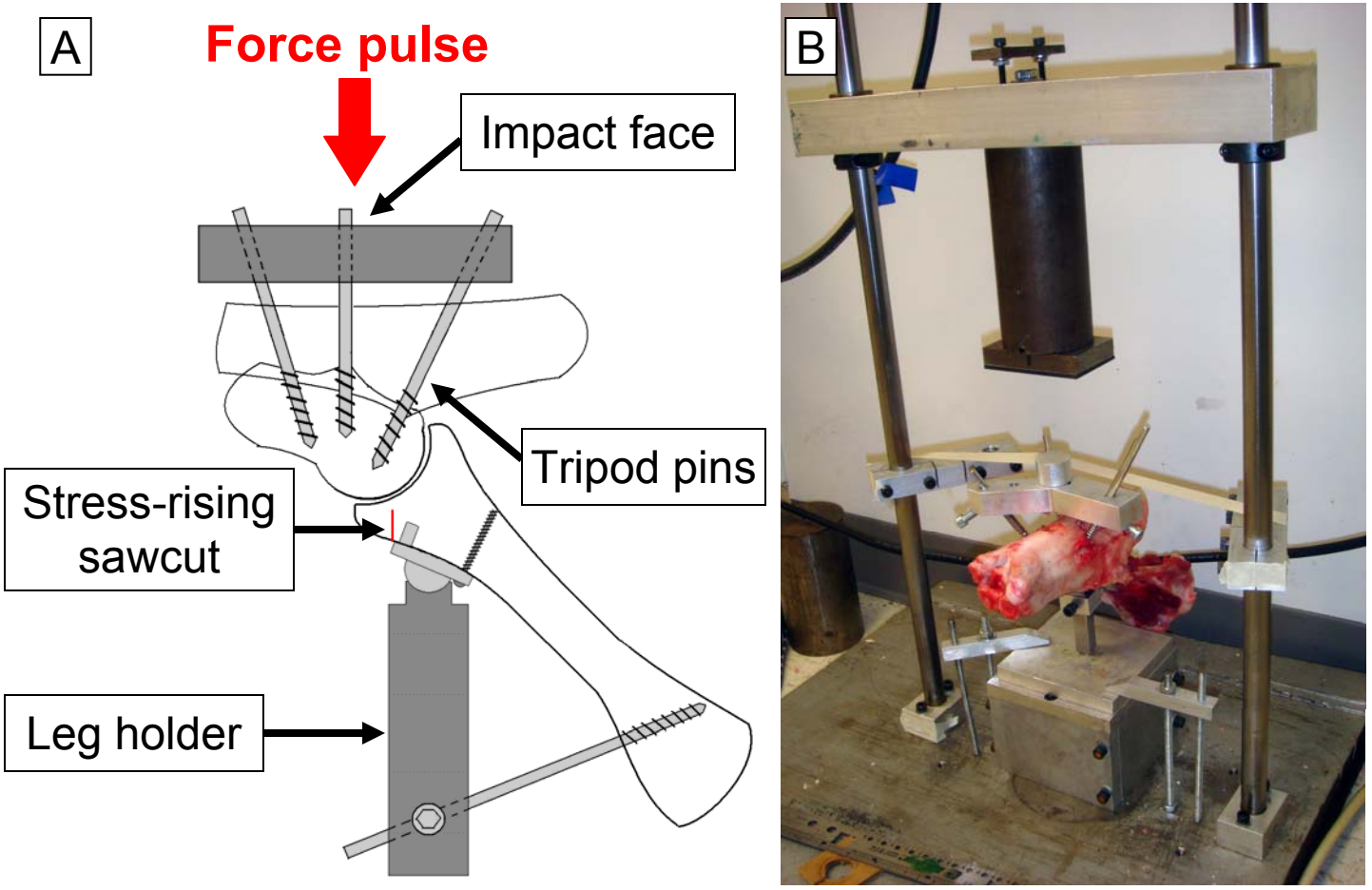

Figure 2
Click here to download Figure: Figure 2R.pdf

Figure 2.

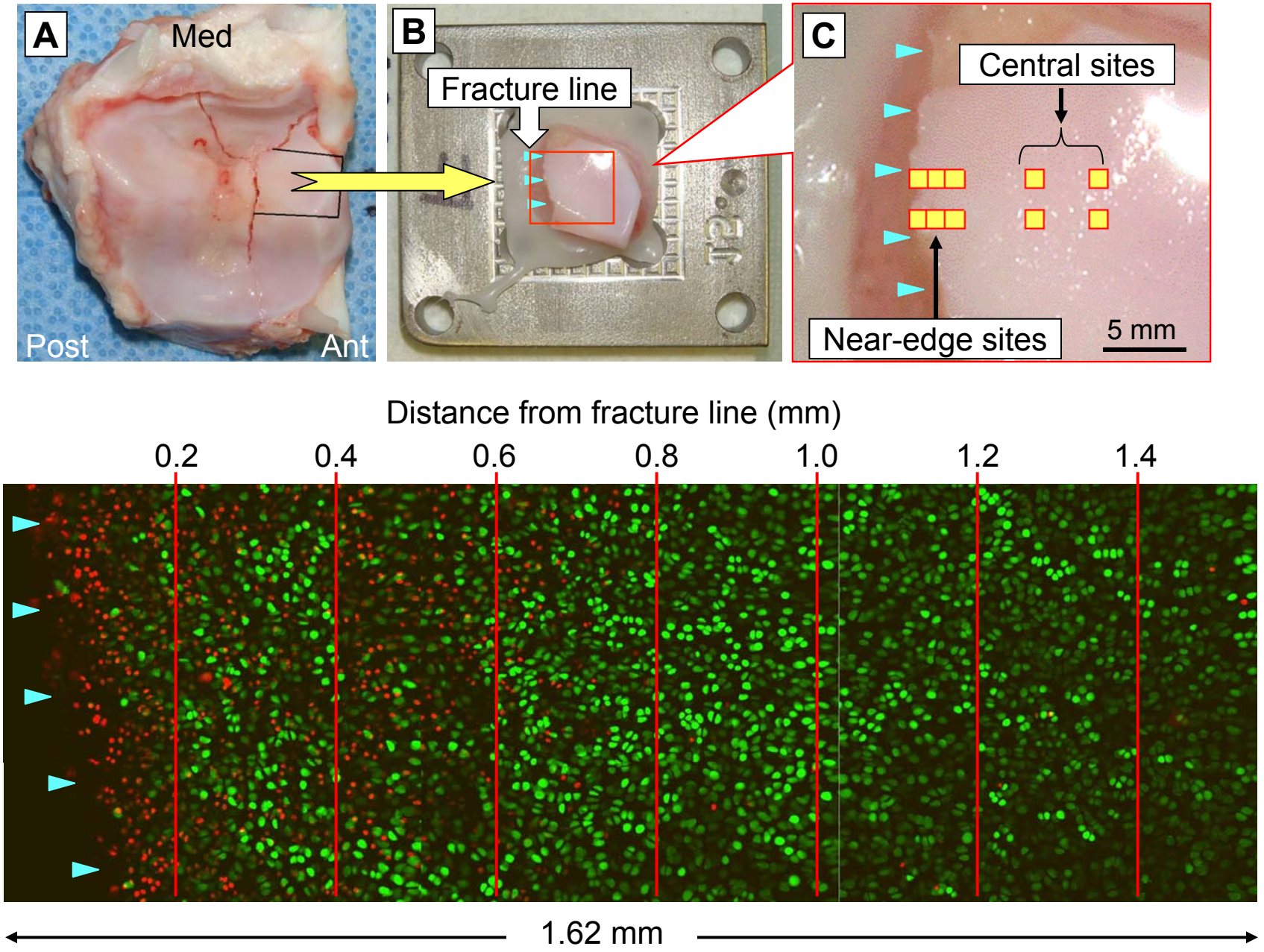

Figure 3
Click here to download Figure: Figure 3R.pdf

Figure 3

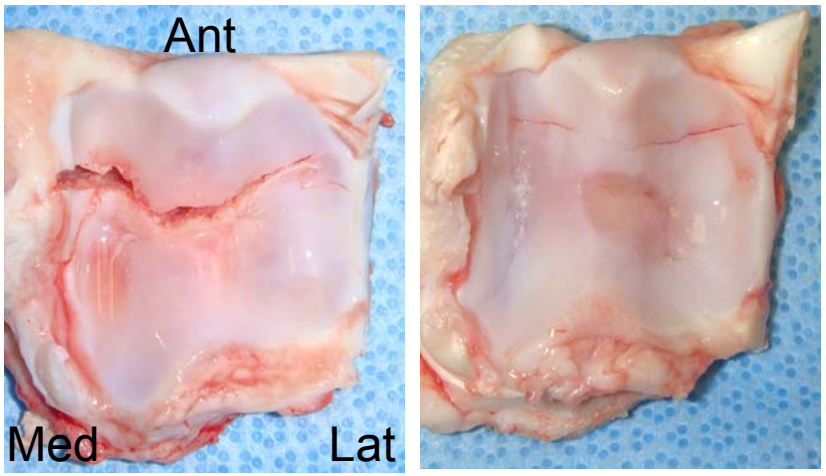

A: Impaction fracture

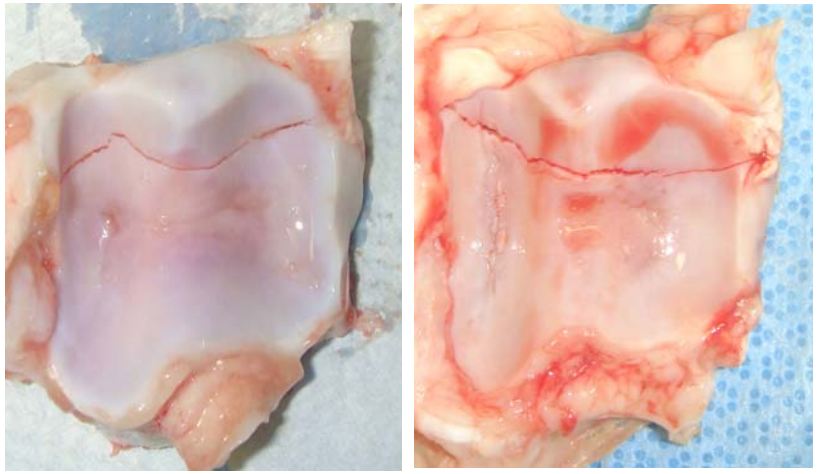

B: Surgical osteotomy

Figure 4

Click here to download Figure: Figure 4R.pdf

Figure 4

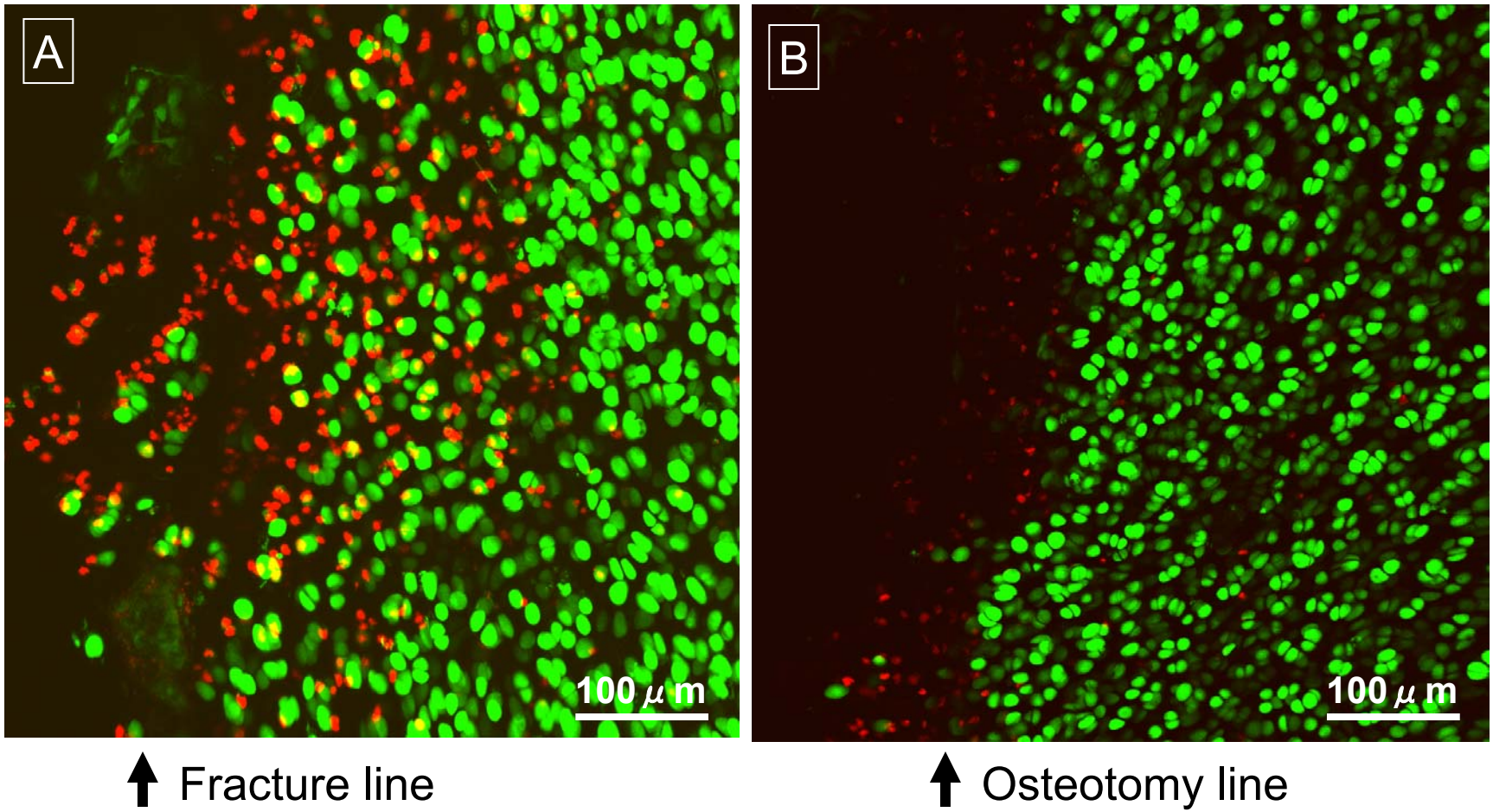

Figure 5

Click here to download Figure: Figure 5R.pdf

Figure 5 (revised)

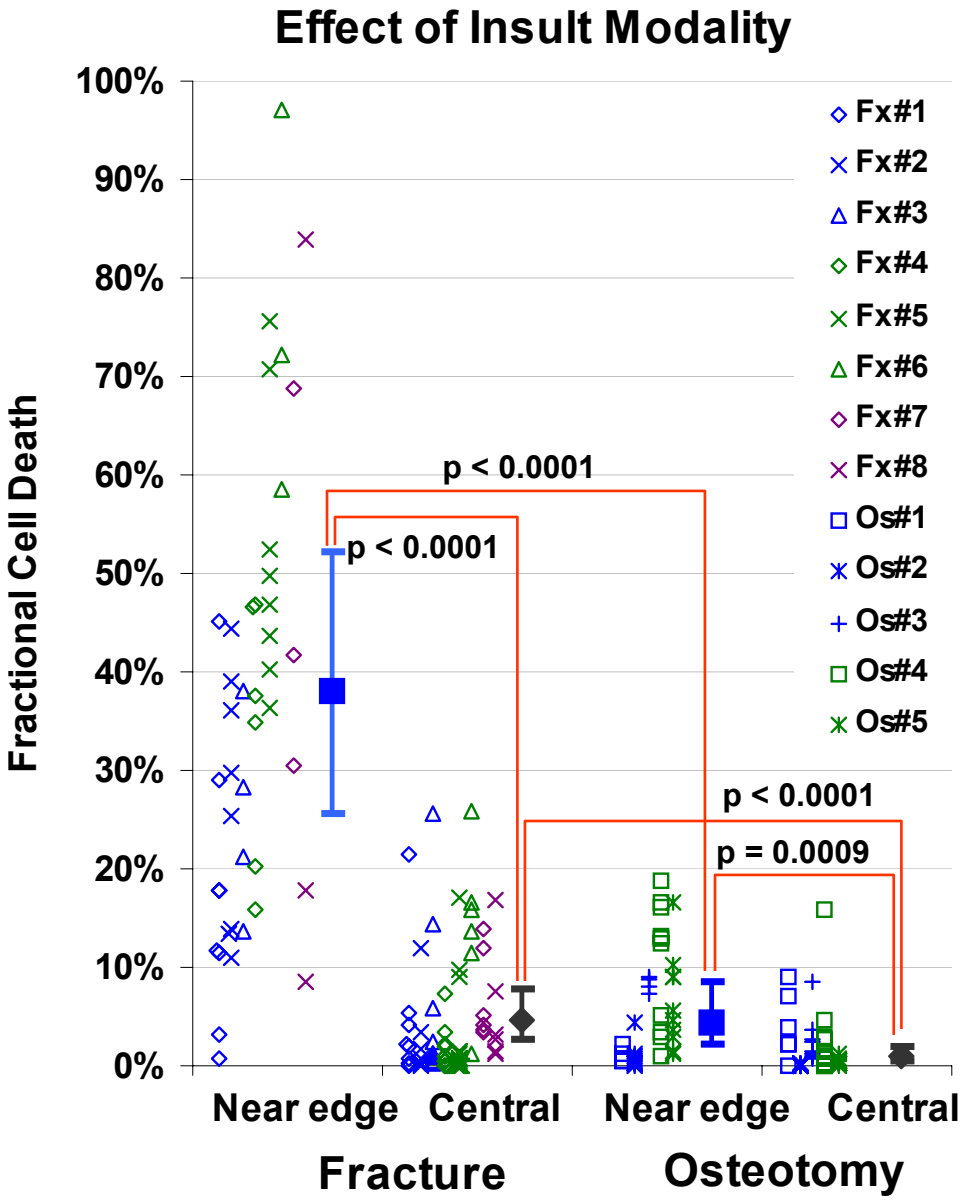

Figure 6

Click here to download Figure: Figure 6R.pdf

Figure 6 (revised)

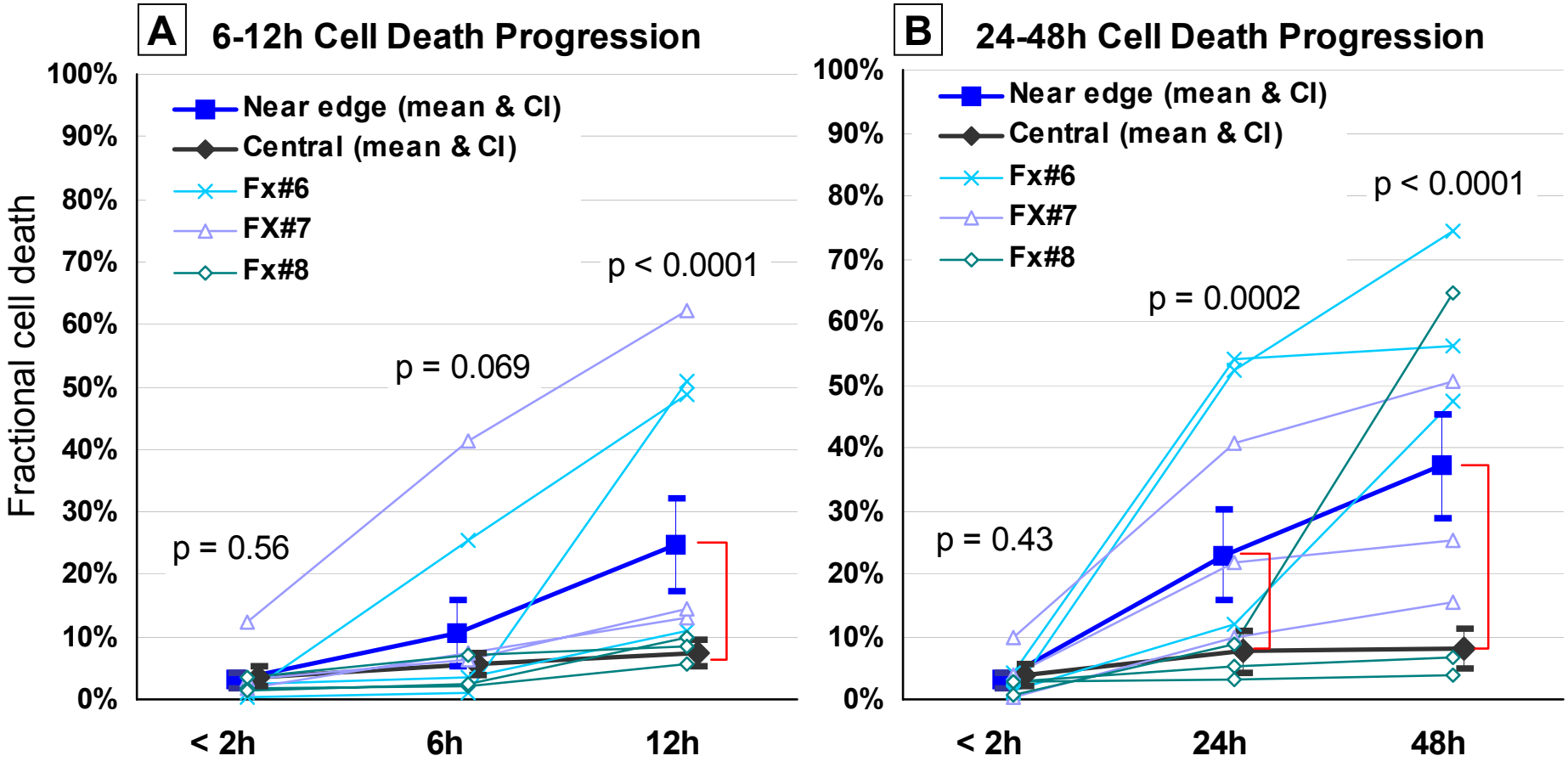

Figure 7
Click here to download Figure: Figure 7R.pdf

Figure 7 (revised)

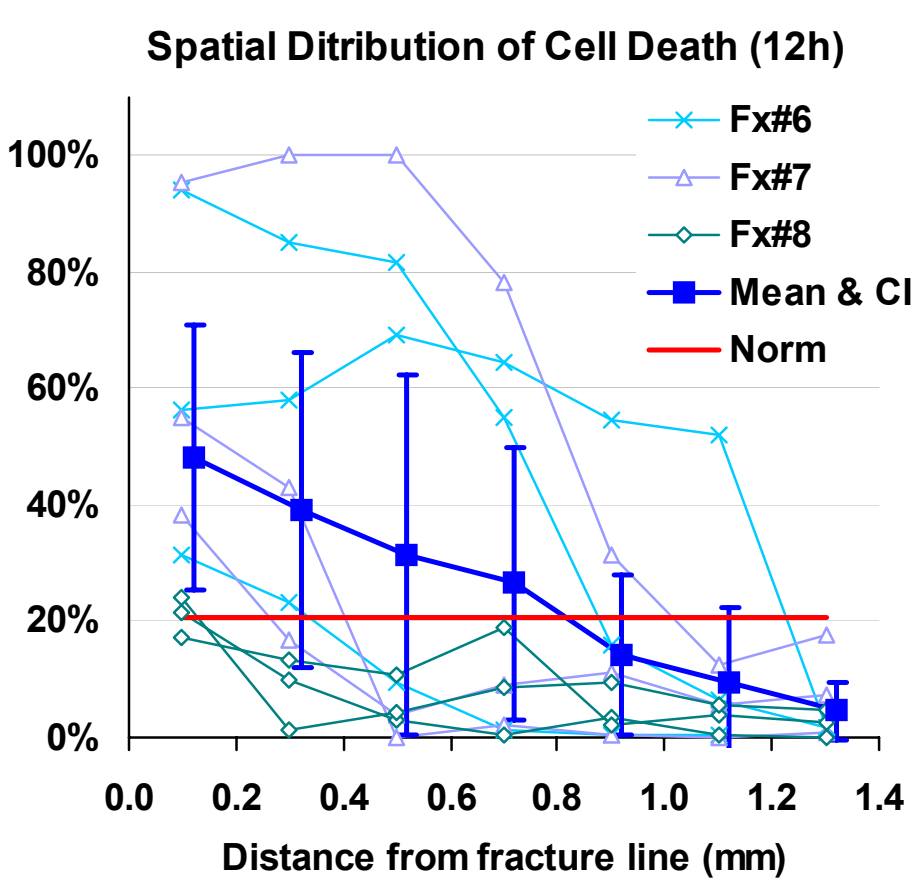

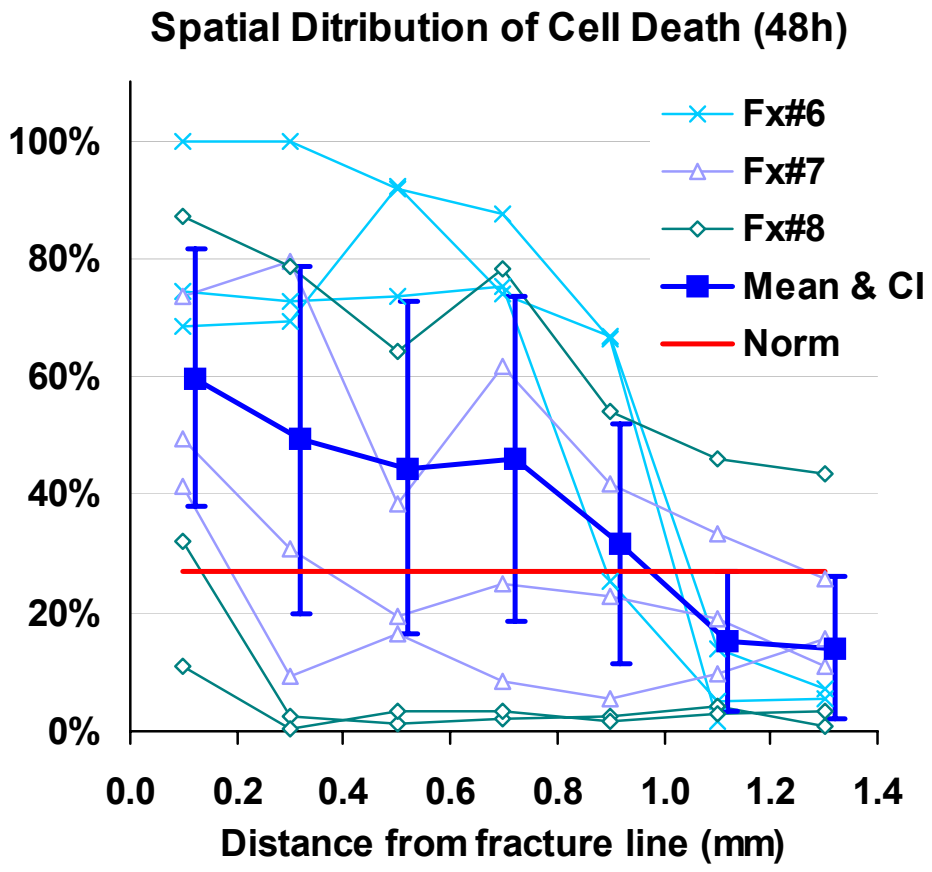

Figure 8
Click here to download Figure: Figure 8R.pdf

Figure 8